To appear in the *Journal of Geophysical Research*, 1995.

The sensitivity of the Martian surface pressure and atmospheric mass budget to various parameters: a comparison between numerical simulations and Viking observations

Frédéric Hourdin, François Forget and Olivier Talagrand
Laboratoire de Météorologie Dynamique du Centre National de la Recherche Scientifique, Ecole Normale Supérieure, Paris, France

Abstract

The sensitivity of the Martian atmospheric circulation to a number of poorly known or strongly varying parameters (surface roughness length, atmospheric optical depth, CO_2 ice albedo, and thermal emissivity) is investigated through experiments performed with the Martian version of the atmospheric general circulation model of Laboratoire de Météorologie Dynamique, with a rather coarse horizontal resolution (a grid with 32 points in longitude and 24 points in latitude). The results are evaluated primarily on the basis of comparisons with the surface pressure records of the Viking mission. To that end, the records are decomposed into long-period seasonal variations due to mass exchange with the polar caps and latitudinal redistribution of mass, and short-period variations due to transient longitudinally propagating waves. The sensitivity experiments include a 5-year control simulation and shorter simulations (a little longer than 1 year) performed with "perturbed" parameter values. The main conclusions are that (1) a change of horizontal resolution (twice as many points in each direction) mostly affects the transient waves, (2) surface roughness lengths have a significant impact on the near-surface wind and, as a matter of consequence, on the latitudinal redistribution of mass, (3) atmospheric dust optical depth has a significant impact on radiative balance and dynamics, and (4) CO_2 ice albedo and thermal emissivity strongly influence mass exchange between the atmosphere and the polar caps. In view of this last conclusion, an automatic procedure is implemented through which the albedo and emissivity of each of the two polar caps are determined, together with the total (i.e., including the caps) atmospheric CO_2 content, in such a way as to get the closest fit of the model to the Viking pressure measurements.

1. Introduction

The meteorology of the planet Mars is probably, after that of Earth, the one which has been most studied and is best understood. This is due, first, to the large number of observations acquired in the seventies on the occasion of several spacecraft missions (the Soviet Mars missions and the American Mariner and Viking missions). In particular, the two Viking landers have recorded near-surface temperature, pressure, and winds over several Martian years. Such records are unique for extraterrestrial planets. The Viking measurements, especially the pressure measurements, contain very instructive information on the global atmospheric circulation. The large-amplitude seasonal oscillations of the pressure are due to the variations of the atmospheric mass (which result from condensation-sublimation of a substantial fraction of the atmospheric carbon dioxide in the polar caps), but also to internal latitudinal mass redistribution. The more rapid oscillations of the surface pressure, with periods of 2 to 5 sols (sols are Martian solar days), are signatures of the transient planetary waves which are present, at least in the northern hemisphere, during autumn and winter. Our relatively good knowledge of the Martian meteorology is also due to the results obtained with atmospheric general circulation models (GCM's). The usefulness of GCM's in this particular instance is certainly due in great part to the similarity of the atmospheric circulations of Earth and Mars. As early as the late sixties, the then recently developed terrestrial GCM of the University of California, Los Angeles, was successfully adapted to Mars [*Leovy and Mintz*, 1969] . The same model, on which various improvements were continuously performed, was later used both for the preparation of the Viking mission and for many studies of the Martian meteorology performed at NASA/Ames Research Center by J. B. Pollack and collaborators [*Pollack et al.*, 1981, 1990, 1993; *Haberle et al.* , 1993; *Barnes et al.*, 1993].

More recently, a new version of the terrestrial GCM of Laboratoire de Météorologie Dynamique (LMD) has been adapted to Mars [*Hourdin*, 1992; *Hourdin et al.*, 1993] . The LMD GCM was the first self-consistent model to simulate the Martian atmospheric circulation over more than a year. Despite the somewhat arbitrary use of an a priori set of model parameters, some of which are poorly known from observation, the model was able to reproduce rather accurately many observed features of the Martian atmosphere, such as the thermal structure derived from Mariner 9 temperature retrievals, and the long- and short-period oscillations of the surface pressure observed by the Viking landers. Moreover, those simulations have shown that the large seasonal pressure variations were not only due, as usually thought until then, to mass exchange between the atmosphere and the polar caps, but were also strongly influenced by internal mass redistribution associated to the atmospheric circulation (*Talagrand et al.* [1991], *Hourdin et al.* [1993], referred to as paper 1 hereinafter, and *Pollack et al.* [1993]).

The present paper, which is a continuation of paper 1, is mainly devoted to sensitivity studies of the LMD model to some very uncertain or strongly varying parameters (surface roughness length, atmospheric optical depth, CO_2 ice albedo, and thermal emissivity) with emphasis on their impact on the atmospheric mass budget and on the meteorological contribution to the annual pressure cycle. Similar studies have already been performed by several authors. *Paige and Ingersoll* [1985], *Wood and Paige* [1992], and *Paige and Wood* [1992] have concentrated on the mass budget with a model of the energetics of the polar caps. *Pollack et al.* [1993] performed a more complete study, since they included in their energy budget model the effect of dynamics (heat transport and meteorological contribution to the pressure variations) using the results of off-line simulations performed with the NASA/Ames GCM on a series of selected short periods. The present work is new in that the sensitivity experiments described here have been performed with a self-consistent GCM allowing for complex feedback between dynamics and diabatic processes.

We try here to answer the following questions: (1) What is the uncertainty in the model resulting from the uncertainties in model parameters or parameterizations? (2) Can the model parameters be constrained from the available observations (and especially from the Viking surface pressure measurements)? (3) What information can be derived from the GCM on the polar processes which dominate the mass cycle?

To that end, we propose simple diagnostics for the Viking pressure measurements, well adapted to the validation of GCMs and to the study of the annual pressure cycle. Those diagnostics are the subject of section 2. We then give in section 3 a brief description of the atmospheric model (already described in paper 1) and present in section 4 a 5-year simulation used afterward as control for the sensitivity experiments. In section 5 we test the uncertainties related to the most uncertain model parameters and, in section 6, we study the impact of the variations of the dust amount in the atmosphere. We take advantage of the high sensitivity of the atmospheric mass budget to the CO_2 ice radiative properties (visible albedo and thermal emissivity) to derive an automatic best fit procedure to the Viking pressure. This procedure and the best fit results are presented in section 7.

2. Analysis of the Viking Surface Pressure Measurements

The records of the surface pressure, acquired over almost 2 Martian years by the Viking 2 lander, and over more than 3 years by the Viking 1 lander [*Tillman and Guest*, 1987] , have been widely used for studies of the Martian transient planetary waves [*Tillman*, 1988; *Barnes*, 1980, 1981], for comparisons with the results of seasonal energy balance models [*Pollack et al.*, 1993; *Paige and Ingersoll*, 1985; *Wood and Paige*, 1992; *Paige and Wood*, 1992] , and, in paper 1, for direct comparisons with GCM simulations. We present here simple diagnostics, well suited to GCM validations, based on a decomposition of the observed variations between a seasonal component (which is itself decomposed into a total atmospheric mass contribution and a meteorological contribution) and a shorter term transient component. In the present paper, which does not discuss diurnal cycle and the associated thermal tides (known to be very strong on Mars), we use directly the diurnally averaged pressure data.

Seasonal Variations

The large-amplitude seasonal variations of the surface pressure can easily be isolated, as proposed by *Tillman et al.* [1993], by retaining the first harmonics of the annual cycle. Following the same authors, we retain only the observations performed after the 1977-B dust storm (clear-sky conditions), but we use solar longitude L_S instead of real time t as the temporal variable of our Fourier analysis. L_S is a more appropriate coordinate for the seasonal cycle, since both the inclination of the planet, $\sin\delta = \sin L_S \sin\delta_0$ (where $\delta_0 \sim 24^o$ is the Martian obliquity), and the distance to the sun, $r = p/(1 + e\cos L_S) \sim p(1 - e\cos L_S)$ (where $p = 1.51$ UA and $e = 0.093$), are almost first harmonics of a year in terms of solar longitude (and not in terms of real time).

The values of the amplitude and phase lag of the first eight harmonics are given in Table 1 for the two Viking landers. The quality of the fit (measured from the root mean square of the difference between the data and the synthetic spectra) reaches a minimum value for $N \geq 5$, the residual value corresponding to the mean amplitude of the transient oscillations (about 0.04 mbar for Viking 1 and 0.1 mbar for Viking 1). Somewhat arbitrarily, the eight-harmonic fit (compared to Viking data in Figure 1) is retained as a reference seasonal pressure cycle in the present study and used for direct comparison with simulated pressures. However, for both landing sites, the first two harmonics explain the main part of the seasonal variations. Note that the two-harmonic fit is much better when solar longitude is used instead of real time as a spectral coordinate. For the time coordi-

Table 1. Amplitude ($p^{(k)}$) and Phase Lag ($L_S^{(k)}$, Solar Longitude of the Maximum Pressure) of the First Eight Harmonics of the Seasonal Pressure Variations Observed by the Viking Landers (Clear-Sky Conditions)

Site	Mode k	$p^{(k)}$, mbar	$L_S^{(k)}$, deg	Mean Quadratic Error ϵ, mbar
VL1	0	7.9623		
	1	0.6887	310.97	
	2	0.5453	66.76	0.0501
	3	0.0154	20.87	0.0512
	4	0.0535	68.53	0.0389
	5	0.0105	33.36	0.0383
	6	0.0053	12.02	0.0378
	7	0.0058	19.85	0.0376
	8	0.0025	13.11	0.0376
VL2	0	8.6889		
	1	0.8320	308.07	
	2	0.6061	66.62	0.1139
	3	0.0422	25.48	0.1120
	4	0.0231	71.05	0.1104
	5	0.0355	65.98	0.1086
	7	0.0119	46.37	0.1081
	8	0.0122	28.59	0.1081

ϵ is the mean quadratic difference between the Viking individual data and the synthetic values reconstructed from the first N harmonics:

$$p^{[N]}(n) = \sum_{k=0}^{k=N} p^{(k)} \cos\left[k \times \left(L_S - L_S^{(k)}\right)\right]$$

nate, for instance, the amplitude of the third harmonic at Viking 1 is of the order of 0.1 mbar, and the root mean square of the difference between the two-harmonic fit and the data is of the order of 0.075 mbar.

As illustrated in Figure 2 and Table 1, harmonic 2 really corresponds to the seasonal cycle with two minima during the two winters, lagging the solstices by about 66^o. The minimum of insolation on one hemisphere at winter solstice corresponds to the maximum condensation rate, the maximum mass of the corresponding cap occurring much later. Harmonic 1 reflects the asymmetry between both winters: mainly forced by orbital eccentricity, it can also be affected by hemispheric asymmetries in orography, in the dust content, and in cloud coverage over caps or amplified by albedo feedbacks on the polar caps. The maximum pressure of the first harmonic also lags the maximum planetary insolation, at perihelion, by about 60^o.

Various Contributions to the Local Seasonal Pressure Variations

As discussed above, the seasonal pressure variations are due in part to the variations of the total atmospheric mass M_{atm} resulting from the mass exchange between the polar caps and the atmosphere. It is convenient to introduce the planetary mean of the surface pressure $p_{\text{atm}} = gM_{\text{atm}}/\left(4\pi a^2\right)$, where a is the planetary radius and g the gravity, and to define in the same way an equivalent surface pressure for the northern and southern polar caps, p_N and p_S respectively, and a total pressure $p_{\text{tot}} = p_{\text{atm}} + p_N + p_S$, which is independent of time.

However, as first pointed out by *Talagrand et al.* [1991], and studied in greater details in paper 1 and by *Pollack et al.* [1993], the seasonal evolution of the surface pressure at a particular point of the planet can differ significantly, under the effect of latitudinal mass redistribution, from the evolution of the mean surface pressure p_{atm}. It is convenient to introduce here the ratio α of the local pressure to the mean atmospheric surface pressure. This ratio will be called the "meteorological factor" hereafter. As shown in paper 1, the horizontal variations of α can be accurately decomposed into the sum of an orographic and a dynamical component. The orographic component (accounting for the horizontal pressure variations along slopes) varies in time because of the strong seasonal variations of temperature. The dynamical component

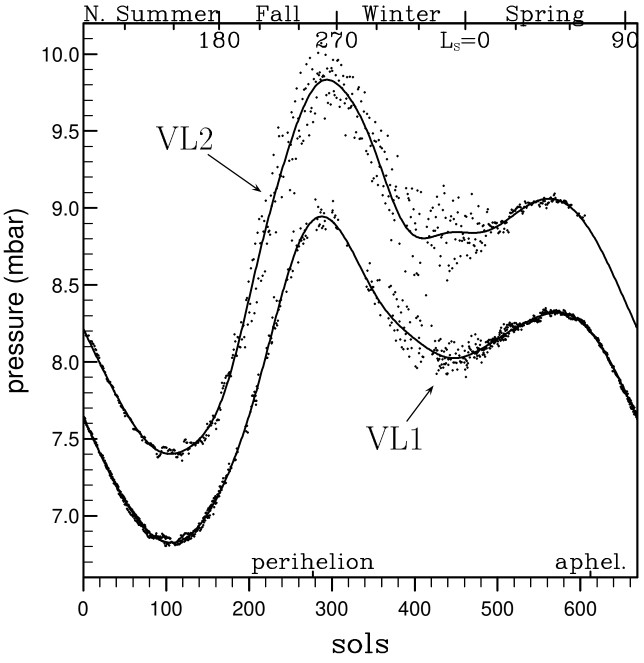

Figure 1. Diurnally averaged Viking pressure observations for clear-sky conditions (points) are compared to the eight-harmonic L_S fit (solid curve).

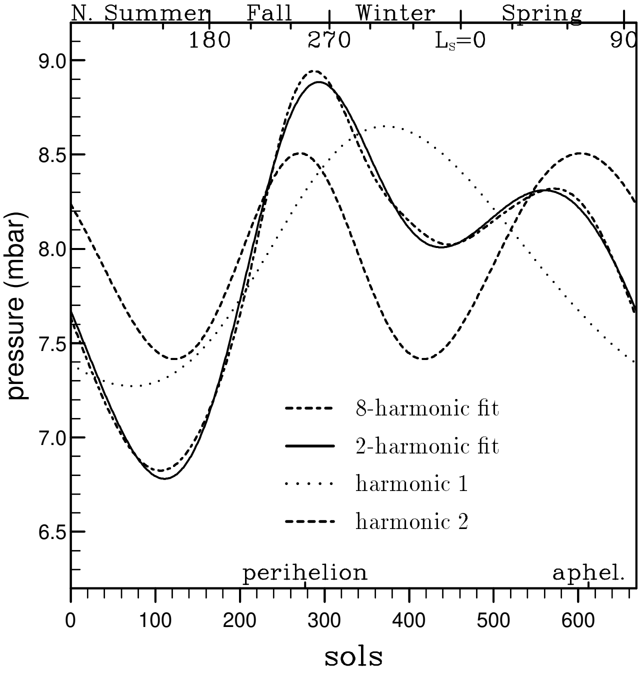

Figure 2. Two- and eight-harmonic fits of the time evolution of the surface pressure observations at Viking 1. The reference eight-harmonic fit is already shown in Figure 1.

is due to the geostrophic balance between the surface pressure and the near-surface horizontal winds. It is particularly responsible for strong latitudinal pressure variations in balance with the strong Martian zonal winds. Those zonal winds are produced themselves by latitudinal angular momentum redistribution by the condensation flow and thermally driven atmospheric circulation.

The absolute meteorological contribution cannot be deduced from Viking observations. However, the relative meteorological factor between the two Viking sites, defined as

$$\alpha_{\mathrm{VL2/1}} = \frac{p_{\mathrm{VL2}} - p_{\mathrm{VL1}}}{p_{\mathrm{VL2}} + p_{\mathrm{VL1}}} = \frac{\alpha_{\mathrm{VL2}} - \alpha_{\mathrm{VL1}}}{\alpha_{\mathrm{VL2}} + \alpha_{\mathrm{VL1}}} \qquad (1)$$

can be used for model validation. Figure 3 shows the relative meteorological factor as computed from the eight-harmonic fits to the Viking 1 and Viking 2 data. The maximum of the curve near northern winter solstice can be explained by the very cold temperatures which strongly enhance the pressure in the lowest Viking 2 site. This effect is partly compensated by the presence of the strong winter jet which should correspond by geostrophic balance to a northward decreasing pressure. As explained in paper 1, the disappearance of the near-surface westerlies during the great 1977-B dust storm ($L_S \sim 280$) was responsible for a sudden increase of the surface pressure recorded by the Viking 2 lander.

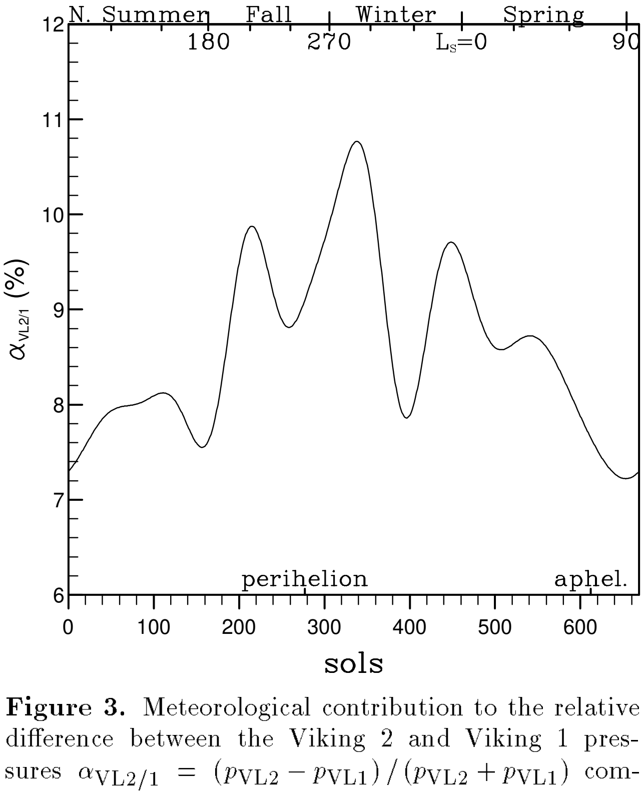

Figure 3. Meteorological contribution to the relative difference between the Viking 2 and Viking 1 pressures $\alpha_{\mathrm{VL2/1}} = (p_{\mathrm{VL2}} - p_{\mathrm{VL1}})/(p_{\mathrm{VL2}} + p_{\mathrm{VL1}})$ computed from the eight-harmonic fits.

It is noteworthy that models must be used in addition to observations of the surface pressure in order to deduce the evolution of the atmospheric mass which requires the knowledge of the absolute meteorological factor. The relative factor $\alpha_{\mathrm{VL2/1}}$ can only help for the model validation.

Transient Eddies

Another important feature of the observed pressure variations is the presence of short-period fluctuations linked to transient planetary waves. Without going into a complete study of these transient waves, which would require the use of more sophisticated analysis techniques, we can easily determine the seasonal evolution of the amplitude of the transient oscillations by retaining the running quadratic mean, σ_N, over N consecutive data, of the difference between the pressure observation for a given sol and the corresponding value computed from the eight-harmonic reference pressure cycle. In order that the seasonal amplitude of the transient waves, but nothing else, be retained in the running mean, the value of N must be significantly larger than the period of the transient waves, and significantly smaller than the length of seasons. As already stated, the analysis is based on diurnally averaged data and thus the transient eddies do not account for the thermal tides.

In Figure 4 we show the time evolution of σ_{25} (thick solid curve) and σ_{50} (dotted curve), which appear to be very similar. For diagnostics, we will retain the eight-harmonic fit to σ_{50} (thin solid line).

Transient eddies occur from northern autumn equinox to early northern spring. The amplitude of the perturbations at the Viking 2 site is about twice that at Viking 1 and shows a two-peak structure with a relative minimum at northern winter solstice.

3. Model

General Description

The LMD Martian GCM has been described in paper 1. The dynamical part is based on a finite difference formulation of the "primitive equations" of meteorology developed for the Terrestrial GCM of LMD [*Sadourny and Laval*, 1984] . We use a more recent formulation (developed by R. Sadourny and P. Le Van and described by F. Hourdin and O. Talagrand, Superrotation of planetary atmospheres: A numerical study, submitted to *Journal of Atmospheric Science*, 1994) which allows us to change automatically the distribution of grid points in longitude and/or latitude. The formulation exactly conserves (1) the total atmospheric mass (in absence of CO_2 condensation), (2) the potential enthalpy and its square for adiabatic motions, (3) the potential enstrophy for barotropic flows, and (4) the total angular momentum for axisymmetric flows.

The physical part has already been presented in detail in paper 1: (1) the radiative transfer is computed using a code adapted by *Hourdin* [1992] from the code currently used at the European Center for Medium-Range Weather Forecasts (ECMWF) [*Fouquart and Bonnel*, 1980; *Morcrette et al.*, 1986] ; it includes absorption and emission by carbon dioxide and dust in the thermal infrared and absorption and scattering by dust in the visible; (2) a simple formulation is used for the vertical turbulent mixing in the whole atmosphere; (3) vertically unstable profiles are prevented by applying a vertical convective adjustment which conserves energy; momentum is also mixed in the unstable layer, the intensity of the mixing depending on the intensity of the vertical instability; (4) the temperature of the surface is computed using an 11–level model of thermal conduction in the soil which correctly simulates the response for oscillatory forcing with periods going from a tenth of day up to a few years; (5) condensation and sublimation of carbon dioxide are computed in a simple energy and mass conserving manner. If somewhere in the atmosphere, the temperature falls below the condensation temperature T_{CO_2}, condensation occurs in an amount appropriate to restore T_{CO_2} by latent heat release. All the condensed CO_2 is assumed to precipitate instantly to the ground, the surface pressure being consequently modified. At the surface, the temperature of the frost is kept at the condensation value either by condensing atmospheric CO_2 or by sublimating CO_2 ice.

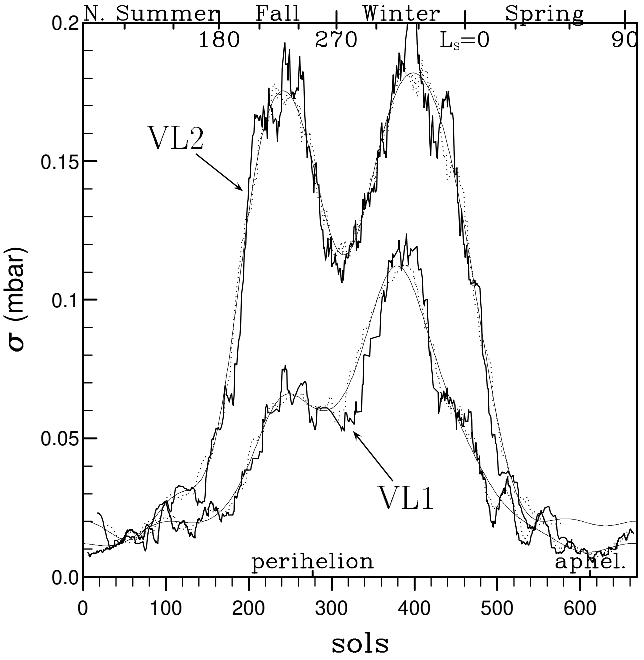

Figure 4. Seasonal evolution of the amplitude of the transient pressure oscillations at both Viking sites computed as the running quadratic mean over 25 (thick solid curve) and 50 (dotted curve) consecutive sols of the difference between the instantaneous (diurnally averaged) Viking pressure and the eight-harmonic fit. The thin solid curve is the eight-harmonic L_S fit to the dotted curve.

The approximation for the pressure-vapor curve used in paper 1 is replaced by a more accurate relationship based on the Clausius-Clapeyron relation for perfect gas. Assuming that the latent heat of sublimation L is independent of temperature, the vapor pressure curve reduces to

$$\ln\left(p/p_0\right) = \frac{L}{R}\left(\frac{1}{T_0} - \frac{1}{T_{CO_2}}\right) \qquad (2)$$

(where R is the gas constant and T_0 is the condensation temperature corresponding to the pressure chosen as a reference, here $p_0 = 1$ mbar). $L = 5.9 \times 10^5$ J kg^{-1} and $T_0 = 136.3$ K are fixed in the range of experimental values [e.g., *James et al.*, 1992] . The change of the pressure-vapor curve was found to have a minor effect on the atmospheric mass budget.

The only significant change with respect to paper 1 is linked to the diurnal cycle. It was intentionally turned off in the previous study. Here, the radiative forcing is computed about 40 times per day. It then becomes necessary to introduce the dependency of the surface drag coefficient (a constant in paper 1) with both the magnitude of wind and vertical stability above the surface which are known to vary significantly between night and day. In the new version, we use the formulation developed by *Louis* [1979] for the terrestrial planetary boundary layer, in the form which has been implemented at ECMWF.

The drag coefficient is given by

$$C = \left(\frac{k}{\ln \frac{z}{z_0}} \right)^2 f \left(R_i, \frac{z}{z_0} \right) \tag{3}$$

where z_0 is the roughness length, z is the height of the middle of the first atmospheric layer, $k = 0.4$ is the von Karman constant, and

$$R_i = \frac{gz\,(\theta - T_s)}{\theta ||V||^2} \tag{4}$$

is the Richardson number, where $\theta = T\,(p_s/p)^\kappa$ and $||V||$ are the potential temperature and wind velocity in the first atmospheric layer and T_s the surface temperature. Two different functions f are used for momentum (f_m) and potential temperature (f_θ). In either case, a different formulation is used, depending on whether the atmosphere is stable ($R_i > 0$),

$$f_m = \frac{1}{1 + 2bR_i/\sqrt{1 + dR_i}} \tag{5}$$

$$f_\theta = \frac{1}{1 + 3bR_i\sqrt{1 + dR_i}} \tag{6}$$

or unstable ($R_i < 0$),

$$f_m = 1 - \frac{3bR_i}{1 + 3bC\left[k/\ln\left(z/z_0\right)\right]^2 \sqrt{-R_i\left(1 + z/z_0\right)}} \tag{7}$$

$$f_\theta = 1 - \frac{3bR_i}{1 + 3bC\left[k/\ln\left(z/z_0\right)\right]^2 \sqrt{-R_i z/z_0}} \tag{8}$$

As in the original terrestrial version, we use $C = b = d = 5$.

Grid

As in paper 1, we use two different horizontal resolutions in the present study: a low horizontal resolution based on a grid with 24 points in latitude and 32 points in longitude and a high resolution with 48 points in latitude and 64 points in longitude. In the vertical, the atmosphere is discretized using 15 σ-levels (σ is the pressure normalized by its surface value $\sigma = p/p_s$), the distribution of which is given in paper 1. The middle of the first layer is located at about 40 m above the surface and the 15th at about 60 km (the pressure is zero at the top of this layer). As pointed out in paper 1, even a coarse horizontal resolution (the low resolution) is sufficient to reproduce, at least qualitatively, the main features of the available observations of the Martian atmospheric circulation. The low resolution was generally retained for sensitivity studies.

Surface Conditions

In addition to the model parameters, three maps are introduced for the surface conditions: orography, visible albedo, and thermal inertia. These maps correspond to the consortium data set, completed by more recent estimation of the surface thermal inertia and albedo in the polar regions [*Keegan et al.*, 1991; *Paige and Keegan*, 1991] , which were provided to us by J. B. Pollack.

4. The Control Simulation

Description

In the present section, we describe a first simulation, which is afterward used as a reference for the sensitivity study. In this "control simulation," the dust visible optical depth is a constant over time and space. Its value is set to 0.2, which corresponds to typical clear-sky conditions [*Martin*, 1986] . Vertically, the dust mixing ratio is almost constant from the surface up to the 0.3-mbar level and then strongly decreases, as proposed by *Pollack et al.* [1990]. The mixing length for vertical turbulent mixing is fixed to 35 m as in the LMD terrestrial GCM. The surface roughness is set to 1 cm everywhere, a value typical of near Viking lander conditions [*Sutton et al.*, 1978] . The emissivity of the bare surface (without ice) is fixed to 0.95, as suggested by *Santee and Crisp* [1993]. The CO_2-ice thermal emissivity ϵ and visible albedo A are set to 0.7 and 0.5, respectively (*Pollack et al.* [1993] have found that those values give reasonable fits to the Viking pressure observations). The dust optical properties are fixed, following *Pollack* [1982], with single-scattering albedo and asymmetry factor in the visible of 0.86 and 0.79, respectively, and a ratio between the absorption efficiency in the thermal infrared Q_{abs}(IR) and extinction efficiency in the visible Q_{ext}(Vis) of 0.2.

As mentioned in paper 1, the interaction between explicitly resolved and unresolved motions is parameterized using an iterated Laplacian acting on the potential temperature and wind components. The operator depends upon one time constant, τ_{diss}, which corresponds to the time of dissipation of the smallest resolved scales. The Laplacian is iterated in order to be more selective in the smaller horizontal scales not acting directly on the large-scale dynamics. Here, the number of iterations n_{diss} is fixed to 2, and τ_{diss} is set to 20,000 s between the surface and the 0.1-mbar level, with rapid decrease to $\tau_{\mathrm{diss}} = 10,000$ s above.

With such values (which were tuned in order to ensure model stability), the characteristic timescale for the parameterized horizontal dissipation is of the order of 0.2 sol for zonal wave numbers $n \sim 12$, of a few sols for $n \sim 6$, and of more than a few tens of sols for $n \leq 3$.

The initial state was taken from an old simulation and, after a phase of stabilization (shorter than one Martian year) due to the modification of model parameters, we simulated 5 consecutive Martian years in order to estimate the interannual variability of the model results, which is of course, crucial for sensitivity studies. For comparison with Viking observations, the simulated surface pressure is interpolated at the two Viking sites from the four closest grid points. The Viking 1 point is somewhat shifted in longitude (from 47.9W to 42.5W) in order to match the currently assumed altitude of the landing site, 1.5 km below the reference altitude of Mars. For Viking 2 (which is generally assumed to be 1 km below Viking 1), since none of the the four closest grid points is below -2 km, the surface pressure is extrapolated downward based on the hydrostatic relationship using the near surface simulated air temperature. As for the Viking observations, the surface pressures are afterward decomposed in terms of seasonal variations and transient eddies. For the seasonal evolution, instead of comparing directly the observed and simulated pressure at the two Viking sites, we present on the one hand, direct comparisons for the Viking 1 site only and use, on the other, the relative pressure difference between Viking 2 and 1 in order to compare the observed and simulated meteorological component.

Viking 1 Pressure

The eight-harmonic fit to the simulated pressure at Viking 1 is reported in Figure 5 (thin solid curves). The interannual variability of the simulated seasonal pressure variations appears to be very weak. The amplitude of the seasonal variations is comparable to Viking 1 observations (dashed curve). This amplitude was somewhat overestimated in the simulations of paper 1. The difference is mainly due to the change of the albedo and emissivity of the polar ice, whereas the introduction of the diurnal cycle (which was tested independently) appears to have a minor effect on the seasonal pressure variations. In the present simulation, the minima and maxima occur approximately at the right seasons. However, a significant discrepancy exists between observations and model, the second pressure maximum being too high in the simulation. The amplitude of the second harmonic is also too large if compared to that of the first harmonic (compare Table 2 for the simulated pressure with Table 1) resulting from an insufficient asymmetry between the two hemispheres.

Planetary Mean of the Surface Pressure

The planetary mean of the surface pressure, p_{atm}, is shown in Figure 6 for the first year of the control simulation, as well as the equivalent pressure of the

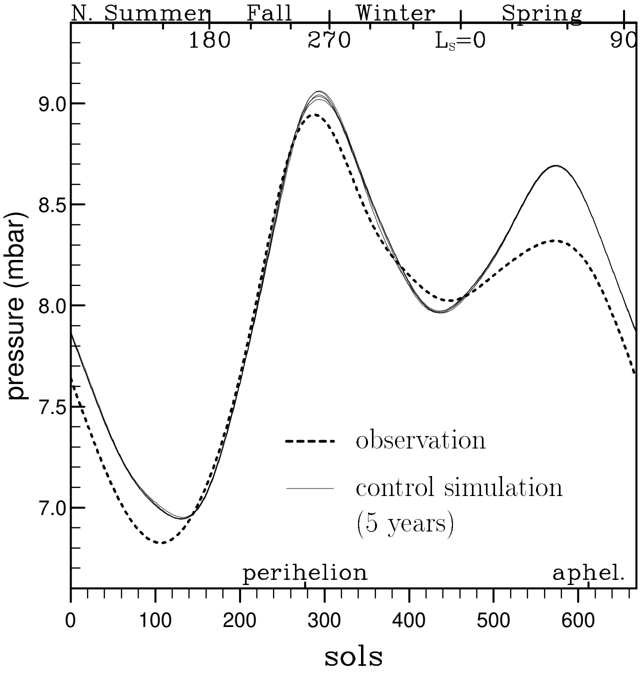

Figure 5. Eight-harmonic L_S fits to the seasonal evolution of the surface pressure at Viking 1. The thin solid curves, almost superimposed, correspond to the five consecutive years of the control simulation. The thick dashed curve (shown in Figure 1) corresponds to Viking 1 observations.

Table 2. Phase Lag (Solar Longitude of the Maximum Pressure) and Amplitude of the First Two Harmonics of the Pressure Seasonal Cycle as Simulated at Viking 1 for the First Year of the Control Simulation

Mode k	$p^{(k)}$, mbar	$L_S^{(k)}$, deg
0	8.063	
1	0.613	320.19
2	0.628	69.87

CO_2 trapped in each cap, p_N and p_S. First, it must be noticed that there is no permanent polar cap in our numerical experiments (this is a common point of most numerical studies of the atmospheric mass budget on Mars). Since the maximum mass of a given cap coincides with a bare pole in the other hemisphere, each pressure minimum really coincides with the maximum mass of the winter cap. The pressure maxima correspond to periods where the two caps are present but very small. The interannual variability of those three curves is very weak and would not be visible on the graph. Thus the small variability in the Viking 1 pressure (Figure 5) is caused almost exclusively by changes in the internal mass redistribution (meteorological component).

Relative Pressure at the Two Sites and Interannual Variability

Figure 7 shows the simulated relative pressure difference between the two landing sites for the five years. The amplitude is in good agreement with Viking observations with a maximum near northern winter solstice and a minimum at southern winter solstice, but high-frequency variations are weaker in the simulation.

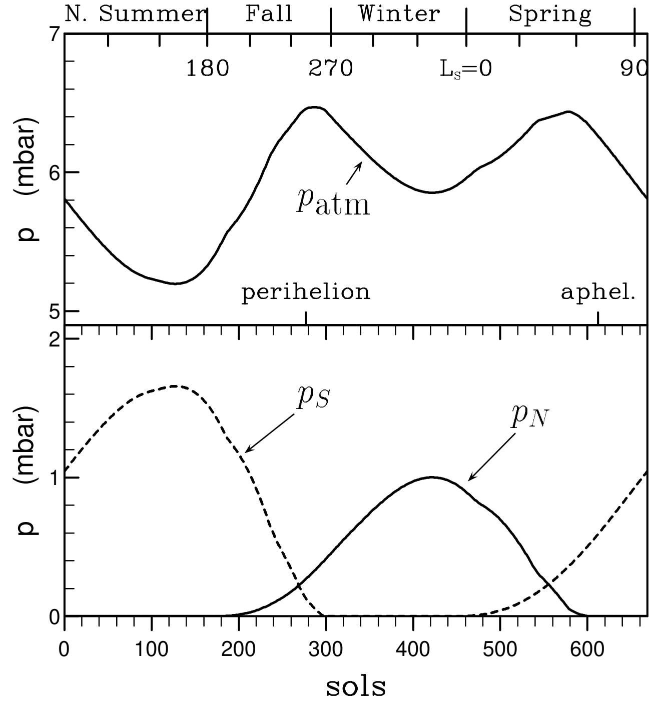

Figure 6. Time evolution of the mean atmospheric surface pressure p_{atm} (upper panel) and that of the equivalent surface pressure of the northern (p_N) and southern cap (p_S) for the first year of the control simulation. The sum of the three components p_{tot} (not shown) does not evolve along seasons and is equal to 6.854 mbar for the control experiment.

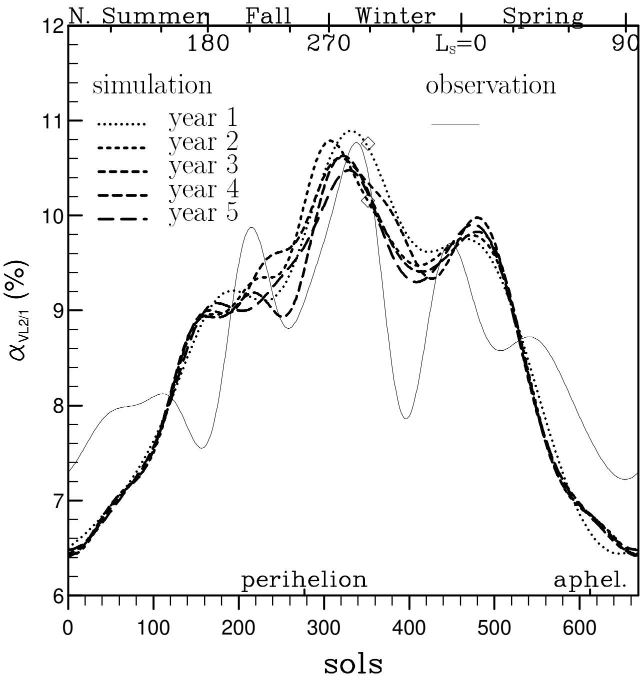

Figure 7. The relative pressure difference between Viking 2 and Viking 1. The thin solid curve (shown in Figure 3) is the observation, and the thick curves correspond to the five successive years of the control simulation.

The simulation shows year–to–year variability but smaller than the discrepancy from Viking data. These interannual variations are due to modifications in the global latitudinal pressure variations. We will concentrate our analysis on the difference between the first and second year of the simulation at $L_S \sim 300$. The corresponding values of $\alpha_{\text{VL2/1}}$ have been marked with diamonds in Figure 7. Relative to the Viking 1 pressure, the Viking 2 pressure is about 0.55% lower in the second year. This is directly related to a change in the zonal wind shown in Figure 8. The upper panel shows the mean zonal wind for the first two years for $L_S = 295$ to 305. We recognize (1) the strong eastward jet in the northern middle and high latitude in geostrophic balance with the strong latitudinal gradient at the edge of the polar cap; (2) the near-surface eastward jet in the southern tropics created, as the Indian monsoon winds on Earth, by transport of angular momentum across the equator in the lower branch of the Hadley cell; and (3) rather weak winds in the rest of the southern hemisphere. The difference between year 1 and year 2 (lower panel) can be interpreted as an equatorward displacement of the winter jet.

The wind in the third layer of the GCM ($p/p_s = 0.966$ and $z \sim 300$ m) is shown for the two years in the upper panel of Figure 9 and the latitudinal pressure variation corresponding to geostrophic balance with this near surface zonal wind is reported in the middle panel of the same figure. The relative difference between year 1 and year 2 of that dynamical component is the solid curve of the lower panel. The corresponding pressure changes at Viking latitudes (22N for Viking 1 and 48N for Viking 2) are compatible with the change in the pressure simulated at Viking sites, which means that these pressure changes are almost totally explained by the modification of the mean zonal winds. Note also the good agreement between the actually simulated pressure modification